

IMECE2018-88676

MULTIPHYSICS MODELING AND PARAMETRIC ANALYSIS OF AN INDUCTOR FOR HEATING THIN SHEET MATERIALS

Alex J. Mazursky

Graduate Researcher

Department of Mechanical and Manufacturing
Engineering, Miami University
Oxford, Ohio 45056

Email: mazursaj@miamioh.edu

Hee-Chang Park

Principal Researcher

Department of Robotics and Mechatronics
Korea Institute of Machinery and Materials (KIMM)
Daejeon, South Korea

Email: hcpark@kimm.re.kr

Sung-Hyuk Song

Senior Researcher

Department of Robotics and Mechatronics
Korea Institute of Machinery and Materials (KIMM)
Daejeon, South Korea

Email: shsong@kimm.re.kr

Jeong-Hoi Koo*

Associate Professor

Department of Mechanical and Manufacturing
Engineering, Miami University
Oxford, Ohio 45056

Email: koo@miamioh.edu

ABSTRACT

Over the past two decades, induction heating technology has begun to replace conventional heating methods in manufacturing due to its ability to rapidly and uniformly heat conductive materials. This advancement has made induction heating very attractive to a wide range of industries, including applications in which thin sheet geometries are used (sheet thickness < 10 mm). According to preliminary testing, conventional coil geometries cannot efficiently heat thin sheet samples. Thus, the primary goal of this study is to investigate a suitable coil design for thin sheet materials and to evaluate the effects of varying coil design parameters. To this end, this project has developed a 3D Multiphysics model that includes a longitudinal induction coil and a thin sheet workpiece. Using the model, a series of parametric studies have been performed to identify the best induction coil geometry for heating of thin sheets along with suitable excitation parameters for the coil and workpiece. It was found that uniform heating is produced when the space between coils is tight. Ad-

ditionally, insignificant variance in temperature uniformity was found when vertically displacing the workpiece within the coil. Parametric studies resulted in finding a cross-section geometry that reduced temperature deviation to within 1.1% across the workpiece width. The model can be used as a design tool for developing a (full-scale) prototype induction heating system.

NOMENCLATURE

<i>A</i>	Magnetic Vector Potential [Wb/m]
<i>B</i>	Magnetic Flux Density [T]
<i>c_p</i>	Specific Heat Capacity [J/kg·K]
<i>D</i>	Electric Displacement [C/m ²]
<i>E</i>	Electric Field [V/m]
<i>H</i>	Magnetic Field Intensity [A/m]
<i>J</i>	Current Density [A/m ²]
<i>Q</i>	Heat [J]
<i>T</i>	Temperature [°C]
<i>t</i>	Time [s]
<i>V</i>	Electric Potential [V]

*Address all correspondence to this author.

<i>Greek Symbols</i>	
δ	Skin Depth [m]
ϵ	Emissivity
λ	Thermal Conductivity [W/m·K]
ρ	Density [kg/m ³]
μ	Permeability [H/m]
μ_0	Permeability of Free Space
μ_r	Relative Permeability
ω	Angular Frequency [rad/s]
σ	Electrical Conductivity [S/m]
σ_{S-B}	Stefan-Boltzmann constant
<i>Subscripts</i>	
amb	Ambient
c	Center
e	External
s	Surface
0	Initial

INTRODUCTION

Induction heating has become increasingly used in recent years for a range of industrial manufacturing processes. It offers numerous advantages over conventional heating techniques (such as flame heating or traditional furnaces): no contact between the heat source and workpiece, fast heating rates, instant controllability, high efficiency, and repeatability and consistency [1–3]. The typical induction heating setup consists of an inductor and a metallic workpiece. The inductor is excited by an alternating current, resulting in a fluctuating magnetic field. In turn, due to Faraday's Law of Induction, eddy currents in opposition to the magnetic field are generated in the workpiece, producing heat through the Joule effect. In addition to heat produced by eddy currents, magnetic hysteresis and residual losses produce heat in ferromagnetic materials.

Proper implementation of induction heating systems has the potential to improve existing manufacturing processes by offering a consistent and cost-effective alternative. In the shoemaking industry, thin adhesive layers are heated using furnaces to activate and join the sole's components [4]. However, in addition to the sole, other pieces of the shoe are subjected to heating in this conventional method, resulting in an overall reduction in shoe quality. In the interest of improving quality of adhesion and reducing manufacturing times, Yun et al. has examined embedding adhesives with conductive particles as a means to locally heat only the adhesive through induction heating [5]. This study experimentally and numerically varied coil geometry, finding induction heating to be a viable alternative, but with work remaining to resolve temperature uniformity.

Similarly, induction heating may yield an economical alternative to traditional processes in tire manufacturing. Current practices use electron beam accelerators to crosslink the rubber

carcass layer for added strength and durability [6–8]. Though accelerators produce effective crosslinking solutions, their capital cost and cost of operation is very high. For tires that have a carcass embedded with ferrous cord, induction heating poses a low-cost and mechanically simpler alternative for the crosslinking of polymers.

These case studies are particularly unique for two key constraints: (1) the workpiece of interest is a thin sheet (thickness < 10 mm) and (2) a uniform temperature across the workpiece width is desired. While previous studies have examined the induction heating of thin sheet geometries using transverse flux and traveling wave inductors, these coil designs cannot produce uniform temperatures without complex, multi-coil design [3, 9–12]. On the manufacturing line, the workpiece may be fed as a long strip along a conveyor through the furnace. To this end, these cases require a uniform temperature across the workpiece width to maintain consistent quality of heating effects in the workpiece.

To address this issue, this paper utilizes a longitudinal coil design, which produces uniform magnetic flux distribution across its width. Specifically, this paper aims to produce a 3D coupled FEM model of an induction heating system for heating thin sheet workpieces. To determine the optimal coil geometry and operating parameters, a series of parametric studies have been conducted.

SYSTEM DESCRIPTION

In the interest of uniform heating, a longitudinal flux coil was used as the basis for the coil geometry, as determined experimentally using the setup shown in Fig. 1 developed by the authors at the Korea Institute of Machinery and Materials (KIMM). In these preliminary experiments, "trial and error" studies were conducted to compare the heating performance of different coil types, cross-section geometries and supplied signals. The work-



FIGURE 1: SETUP OF INDUCTION HEATING EXPERIMENTS TO MEASURE EFFECT OF COIL GEOMETRY ON WORKPIECE TEMPERATURE DISTRIBUTION.

piece was fitted with thermocouples to record the temperature at different locations over time. It was concluded that for thin sheet materials, a rectangular cross-section is most effective at producing a uniform temperature distribution in the workpiece, compared to conventional circular or stadium cross-sections. To further improve the efficiency of the system, the inductor design should be “optimized.” Thus, the present computational study intends to investigate a longitudinal, rectangular-shaped coil with a thin workpiece placed inside. The experimental results obtained by the system are used as the basis for the current computational study.

MATHEMATICAL MODEL

This section describes the simulation model used to numerically evaluate the induction heating process. The induction heating process can be estimated using the finite element method and a multiphysics coupling between the magnetic field equations in the frequency domain and the heat transfer equations in the transient domain.

As shown in Fig. 2, the model geometry, material designation, initial and boundary conditions, forcing functions and domain discretization are all defined in pre-processing. When the solver runs, it first solves for the magnetic fields within the frequency domain using Maxwell's equations. The heat produced by the electromagnetic phenomena is then handled in transient time within the heat transfer module. A temperature coupling is used to feed temperature dependent parameters back into the frequency solver for the next time step. The coupled solver finishes when a specified final time or temperature value is reached. In post-processing, many other variables may be analyzed, such as induced power and radiation loss.

Electromagnetic Model

Upon defining the pre-processing parameters, the model solves Maxwell's equations in the frequency domain beginning with the magnetic vector potential:

$$\vec{B} = \nabla \times \vec{A} \quad (1)$$

where $\vec{B}(\vec{H})$ is given by the constitutive relation:

$$\vec{B} = \mu_0 \mu_r \vec{H} \quad (2)$$

The Maxwell-Ampere equation is given by:

$$\vec{J} = \nabla \times \vec{H} \quad (3)$$

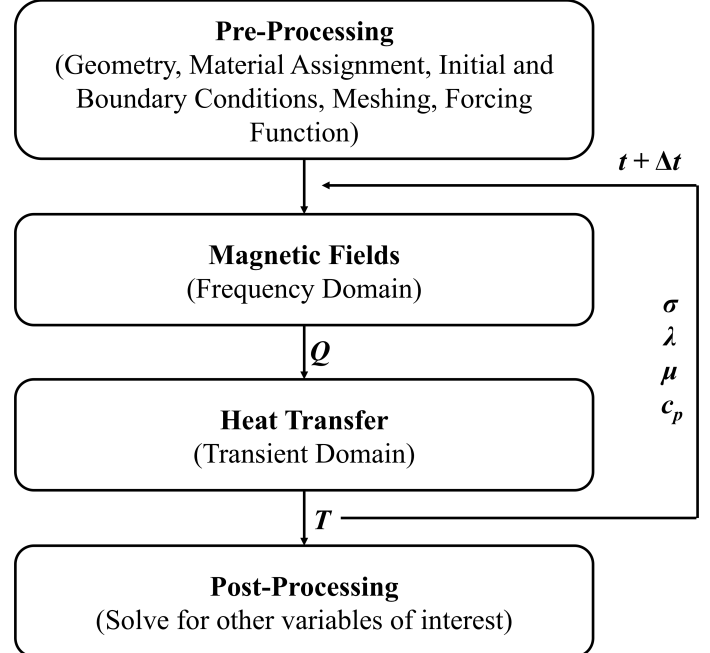


FIGURE 2: SIMULATION PROCESS FOR SOLVING THE INDUCTION HEATING PROBLEM.

where the current density may be represented as a constitutive relation:

$$\vec{J} = \sigma \vec{E} + \vec{J}_e + j\omega D \quad (4)$$

The Maxwell-Faraday equation is given by:

$$\nabla \times \vec{E} = - \frac{\partial \vec{B}}{\partial t} \quad (5)$$

where electric field is defined as:

$$\vec{E} = -j\omega A \quad (6)$$

The Joule loss due to the induced eddy currents in the workpiece can be written as:

$$Q = \frac{(\text{Re}(J_e))^2}{\sigma} \quad (7)$$

and carried into the heat transfer model for transient analysis.

Heat Transfer Model

Within the heat transfer model, the energy produced through Joule losses is treated as a heat source. The process can be described by the heat equation:

$$Q = \rho c_p \frac{\partial T}{\partial t} + \rho c_p u \cdot \nabla T - \nabla(\lambda \nabla T) \quad (8)$$

In this model, the workpiece's temperature at the current time step is evaluated. Within the model, a stop condition was implemented for when the center of the workpiece reached the desired temperature.

METHODS OF ANALYSIS

The induction heating system was modeled as a scalable 3D FEM problem in COMSOL® Multiphysics 5.3. The coil and workpiece schematic is shown in Fig. 3 and was modeled after an experimental setup developed at KIMM. To supply power to the coil, a lumped port boundary was applied at the coil junction to act as a current source. The modeled system was surrounded by an infinite element air domain. The dimensions of the coil and workpiece are detailed in Tab. 1. The material parameters of the studied system are given in Tab. 2. The workpiece was modeled as homogeneous and smooth. Air has been assigned a small electrical conductivity for numerical stability. A number of additional assumptions were used in defining the model and are detailed below.

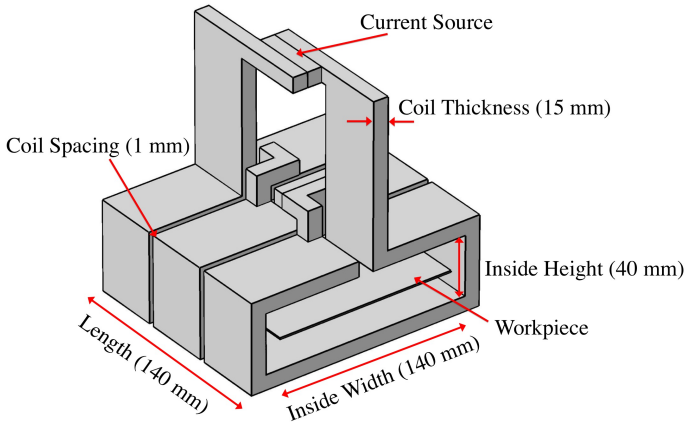


FIGURE 3: 3D MODEL GEOMETRY.

Though not a governing equation, the skin depth must be carefully considered in induction heating processes. The skin depth of the induced current is defined as the depth below the conductor surface at which the current density J has decreased by

TABLE 1: DIMENSIONS OF THE INDUCTION COIL AND WORKPIECE.

Induction Coil	Description	Workpiece	Description
Material	Copper	Material	Iron
Length	140 mm	Length	120 mm
Inside Width	140 mm	Width	90 mm
Inside Height	40 mm		
Thickness	15 mm	Thickness	1 mm
Number of Turns	3		
Spacing	1 mm		

TABLE 2: MATERIAL PROPERTIES OF THE INDUCTION HEATING MODEL.

	Copper	Iron	Air
c_p	385	440	1.003
ϵ		0.77	
λ	400	76.2	1.4
ρ	8700	7870	1.225
μ_r	1	4000	1
σ	5.99×10^7	1.12×10^7	1

a factor e^{-1} of the surface current J_s . If the skin depth is large relative to the size of the workpiece, the heat source density may be taken to be uniform throughout the sample. However, for smaller skin depths, the majority of the heat production would take place on the workpiece surface and conduct inward. The skin depth may be approximated:

$$\delta = \sqrt{\frac{2}{\omega \mu \sigma}} \quad (9)$$

Because of the workpiece's thin geometry in this study, a high excitation frequency was used. At higher order frequencies, the skin depth becomes significantly smaller than the size of the object. For instance, at 240 kHz, the skin depths of copper and iron are found to be 0.133 and 0.005 mm, respectively. Compared to the thickness of the coil and workpiece, these depths are small enough to be approximated as flowing on the system's surfaces by applying an Impedance Boundary Condition. There-

fore, significant computational time may be saved by avoiding thin, boundary layer meshing within the model.

Within the heat transfer domain, a diffusive boundary condition was applied to the workpiece's surfaces and edges, which followed the surface-to-ambient radiation equation:

$$\frac{Q}{A} = \epsilon \sigma_{S-B} (T_{amb}^4 - T^4) \quad (10)$$

where σ_{S-B} is the Stefan-Boltzmann constant.

A mesh convergence study was performed to determine the appropriate mesh size and distribution. Specifically, the convergence study focused on the coil's mesh due to the greater computational demand of solving the frequency problem compared to the transient. The results are shown in Fig. 4. A compromise was made between the number of elements in the last two points for the investigated model.

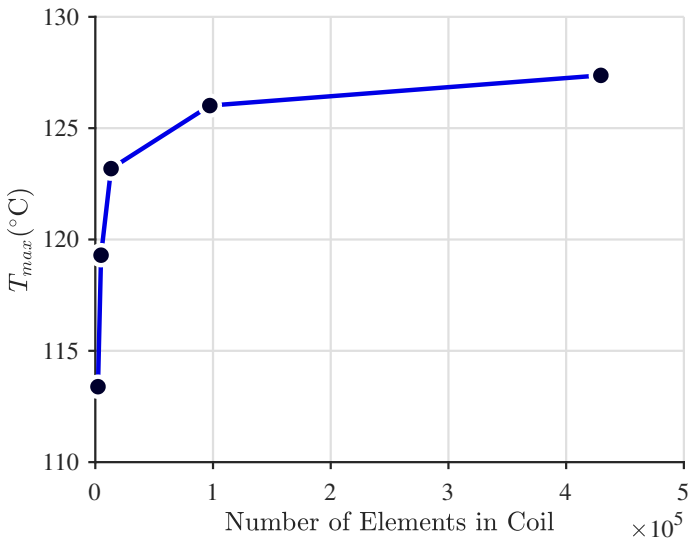


FIGURE 4: INVESTIGATION OF EFFECTS OF MESH SIZE IN THE COIL ON MAXIMUM TEMPERATURE IN THE WORKPIECE, $t = 20$ s.

The investigated model was assigned the mesh shown in Fig. 5. The mesh density was greatest near the coil's gaps to properly approximate electromagnetic phenomena. The workpiece geometry was meshed densely, especially along the edges to ensure resolution of edge effects.

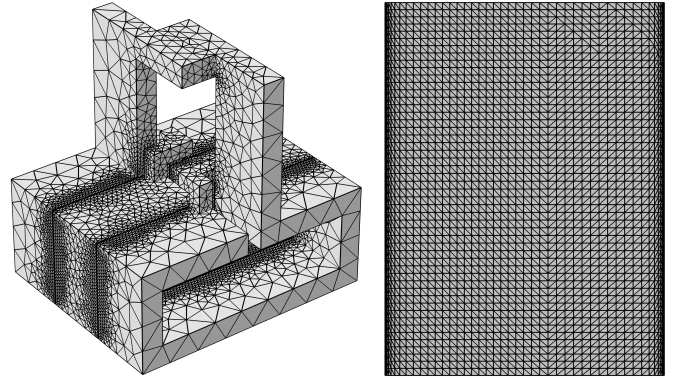


FIGURE 5: FINITE ELEMENT MESH APPLIED TO THE COIL AND WORKPIECE.

SIMULATION RESULTS AND DISCUSSION

The results produced by the model are presented in this section. The model was first validated by following procedures similar to experiments performed with a physical system. Following validation, design analysis was performed on the coil's geometry and operating parameters. The goal of this analysis was to determine the effects of varying coil design parameters on the temperature distribution in the workpiece. A uniform temperature of 120°C across the width of the workpiece was chosen as the performance metric, representing the melting temperature of a typical adhesive used in shoemaking.

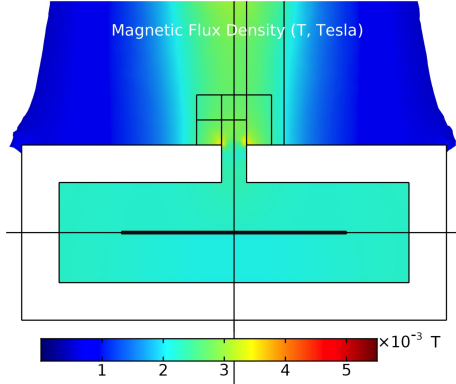
Baseline Evaluation

The model was first tested using excitation parameters based upon parameters used in parallel experiments at KIMM. The results of this initial study are used to form the baseline of comparison for all following tests. The baseline geometry is presented in Tab. 1 and the baseline excitation parameters are presented in Tab. 3.

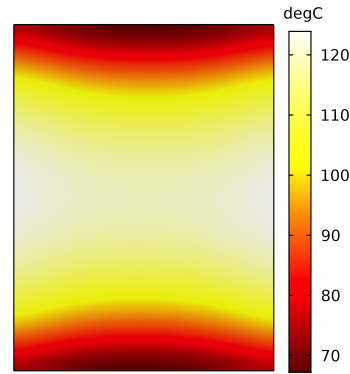
TABLE 3: PROCESS PARAMETERS.

Quantity	Value
Current	92 A
Frequency	240 kHz
t	$t(T_c = 120^\circ\text{C})$
T_0	20°C
T_{amb}	20°C

The model was solved using the baseline parameters. To



(a) SLICE PLOT OF THE MAGNETIC FLUX DENSITY (T) ACROSS THE COIL'S CROSS-SECTION AT MID-LENGTH.



(b) SURFACE TEMPERATURE OF THE IRON WORKPIECE WHEN $T_c = 120^\circ\text{C}$.

FIGURE 6: CONTOUR PLOTS PRODUCED BY THE BASELINE MODEL PARAMETERS.

verify that the coil's design was operating as expected, the distribution of the magnetic flux density (T) was investigated. A slice plot of the magnetic flux density halfway along the coil's length is shown in Fig. 6a. Inside the coil, the magnetic flux density is nearly uniform at about 2.2×10^{-3} T. The flux uniformity is a product of the longitudinal coil design.

The temperature contour of the workpiece's surface is shown in Fig. 6b for when the center of the sheet has reached the desired central temperature $T_c = 120^\circ\text{C}$. At the midpoint of the workpiece's length, the temperature profile is nearly uniform across its width. This is due to the nature of the uniform flux produced by selecting a longitudinal coil. However, edge effects are observed in the form of overheating along the lengthwise edges and underheating along the widthwise edges. In the context of the manufacturing line, the workpiece may travel along the length of the coil, perpendicular to the planes formed by the workpiece width and thickness. Therefore, any slice of the workpiece along its length may be subjected to similar magnetic flux conditions as all other slices along the workpiece length. However, this assertion does not apply to slices bounded by the workpiece length and thickness, as this plane is parallel to the workpiece's velocity. Therefore, this study uses temperature along the workpiece width as the metric for uniform heating.

The temperature distribution across the iron workpiece's width was normalized about T_c to show the percent change in temperature relative to the temperate at the center, as shown in Fig. 7. By normalizing the temperature distributions with respect to T_c and applying symmetry, the initial resultant distribution may be used as a baseline with which to compare future tests. The baseline examination found there to be about 3.7°C difference between the center and edge temperatures, or a percent difference of 3.08%.

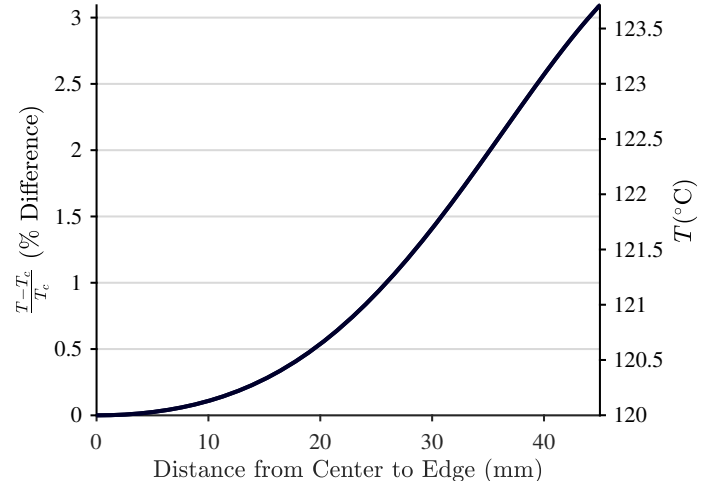


FIGURE 7: NORMALIZED TEMPERATURE DISTRIBUTION FROM CENTER TO EDGE.

Effect of the Spacing Between Coils

The first parameter examined was the effect of varying the distance between the coils. The spacing was varied from 1 to 30 mm. The total length of the coil was fixed at 140 mm and the supplied power was held constant at 8.5 kW by adjusting the current for the impedance of each coil for proper comparability. The normalized temperature distribution across the sheet's width is presented in Fig. 8 and the time history plot of the temperature at the workpiece center is shown in Fig. 9. It can be seen that as the distance between the coils increased, the temperature gradient became steeper, with 1 mm spacing resulting in the smallest percent difference.

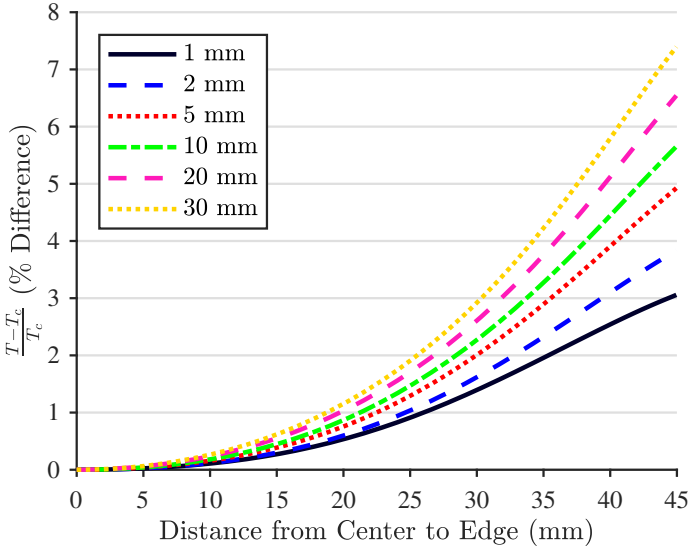


FIGURE 8: NORMALIZED TEMPERATURE DISTRIBUTION FROM CENTER TO EDGE FOR VARIOUS COIL SPACING.

However, the time to reach $T_c = 120^\circ\text{C}$ was slower for coils with tighter spacing. A 1 mm coil spacing produced the desired T_c in 19.7 s, while a 30 mm coil spacing reached 120°C in 7.9 s. Therefore, the apparent trade-off between temperature uniformity and time to heat must be considered when deciding the spacing between coils.

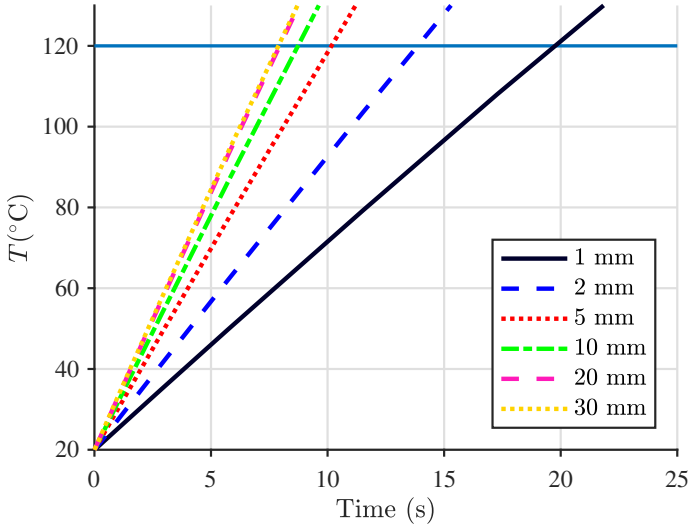


FIGURE 9: TEMPERATURE AT THE WORKPIECE CENTER OVER TIME FOR VARIOUS COIL SPACING.

Effect of Workpiece's Vertical Position

Many applications of thin sheets are not entirely flat geometries. For instance, the soles of shoes have a “heel-to-toe drop,” or a difference in height between the heel and forefoot position. Similarly, belt-driven assembly lines may have a degree of z-axis variation. To test the degree of the longitudinal coil design’s robustness to handle variations in vertical position, the workpiece’s position was offset 10 mm along the z-axis. The standard coil geometry and operating parameters, shown in Tabs. 1 and 3, was used for this analysis, which is presented in Fig. 10. It was found that for the greatest negative z-displacement, -10 mm, a maximum of 4.6% degrees of overheating was expected in the workpiece. When the workpiece was displaced by 10 mm in the positive z-direction, about 0.49% underheating was observed 22.5 mm outward from center of the workpiece. Compared to the case of 0 mm offset, a maximum temperature difference of about $\pm 2.0\%$ was observed.

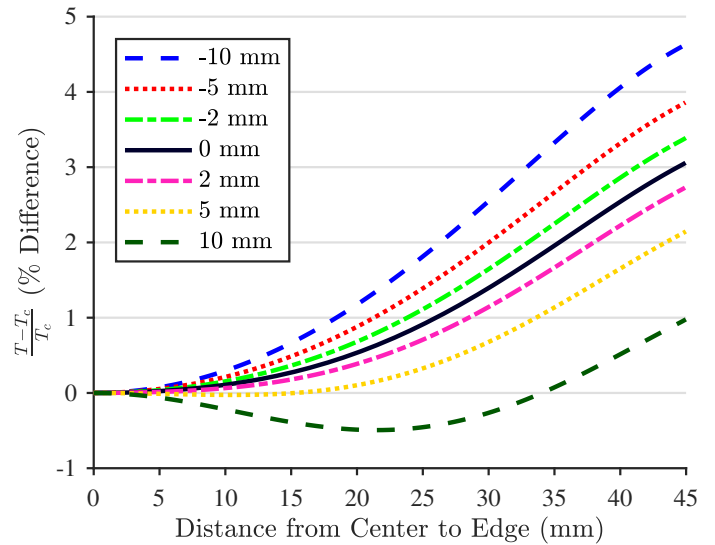


FIGURE 10: NORMALIZED TEMPERATURE DISTRIBUTION FROM CENTER TO EDGE FOR WORKPIECE Z-DISPLACEMENTS.

Effect of the Coil's Cross-Sectional Geometry

To mitigate overheating along the sheet’s edges, the effect of varying the inside height and width of the coil on temperature distribution was examined. As the distance between the inductor and workpiece decreases, it is expected that the rate of heat generation will due to the increased strength of the proximity effect.

The inside width of the coil was varied from 100 to 220 mm and the supplied power was held constant at 8.5 kW by adjusting the current for the impedance of each coil for proper comparability. As shown in Fig. 11a, for coil widths less than 140 mm, the

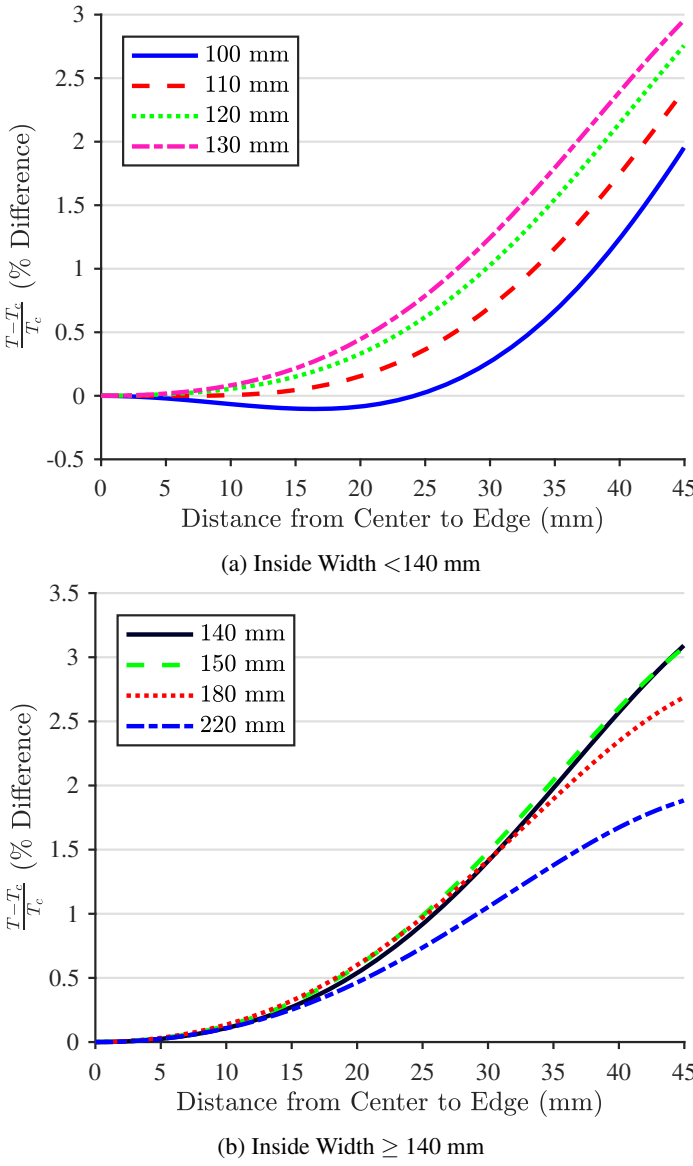


FIGURE 11: NORMALIZED TEMPERATURE DISTRIBUTION FROM CENTER TO EDGE FOR VARIOUS COIL WIDTHS.

temperature distribution was concave upward and became more uniform as the width decreased. However, for coil widths greater than 140 mm, the temperature profile near the edge of the workpiece changed concavity as width increased. For lesser widths, there are combined proximity effects from both sides of the coil, resulting in a more uniform temperature. For greater widths, the proximity effect has less influence and also results in a homogeneous temperature.

Similarly, the inside height of the coil was varied from 10 to 80 mm at a constant power of 8.5 kW by adjusting the sup-

plied current. The width of the coil was kept at 140 mm. Fig. 12 shows the effect of adjusting the coil height on temperature distribution across the workpiece width. Again, it was found that for shorter distances between the coil and workpiece, the temperature distribution was concave upward. As the height increased, the temperature gradient near the workpiece edge decreased. For heights below 30 mm, the workpiece was underheated across its width until nearing the edge affected zone.

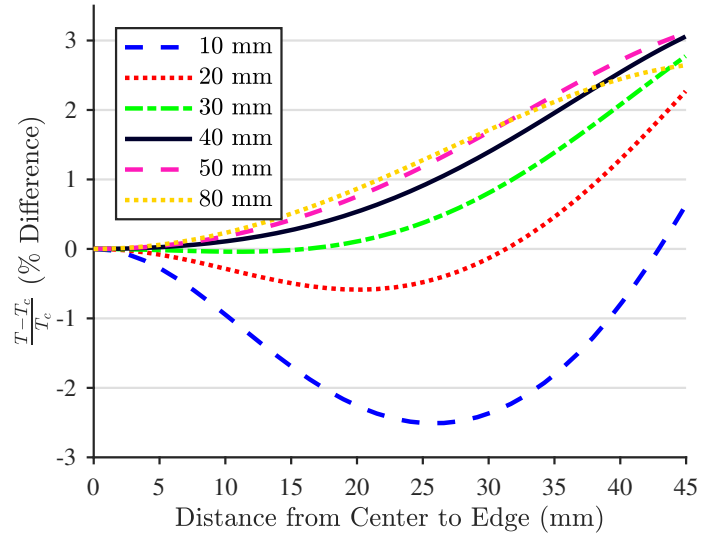


FIGURE 12: NORMALIZED TEMPERATURE DISTRIBUTION FROM CENTER TO EDGE FOR VARIOUS COIL HEIGHTS.

Toward Optimal Geometry

In previous sections, only one parameter was varied at a time. For a more robust refinement toward uniform temperature distribution, this section evaluates for the effects of varying both coil width and height. The range of dimensions investigated was chosen based upon the results of the previous section. The widths tested were 100, 105 and 110 mm, while the heights examined were 20, 25 and 30 mm. All combinations of the widths and heights were compared and the resultant distributions and time history plots are presented in Fig. 13 and Fig. 14, respectively. In this study, the spacing was fixed at 1 mm in favor of uniform heating compared to rapid heating. The workpiece was centered within the coil. The excitation parameters are given in Tab. 3.

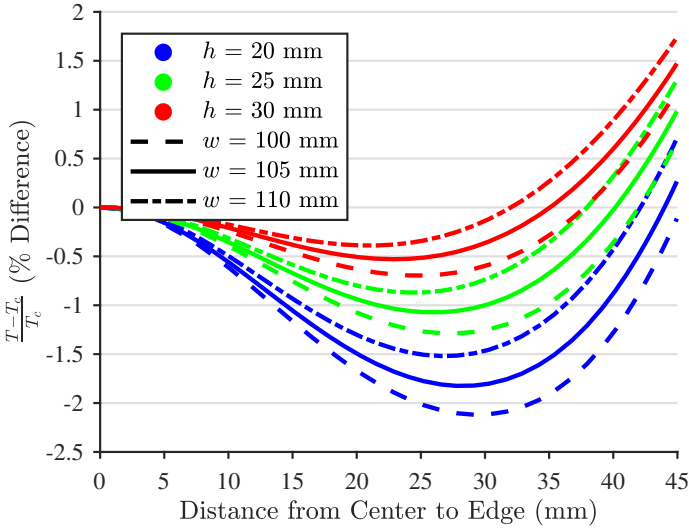


FIGURE 13: TEMPERATURE DISTRIBUTION FROM CENTER TO EDGE FOR VARIOUS CROSS-SECTION DIMENSIONS.

It can be seen that the effect of varying the coil height by 5 mm tends to outweigh the effect of varying the coil width by the same amount. The cross-section geometry that resulted in the lowest temperature deviation from the desired value was 105 mm wide and 25 mm tall. The deviation was below $\pm 1.1\%$ across the width of the workpiece, about 1.9% less than that of the baseline result.

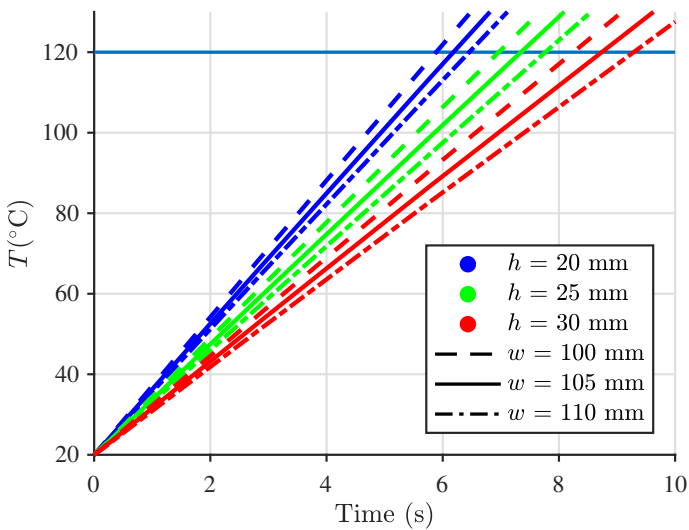


FIGURE 14: TEMPERATURE AT THE WORKPIECE CENTER OVER TIME FOR VARIOUS CROSS-SECTION DIMENSIONS.

It is also evident that as the height and width increase, the time to heat to $T_c = 120^\circ\text{C}$ increases as well. The cross-sections examined resulted in time savings of up to 70% from the baseline results, despite operating under the same input power and frequency.

CONCLUSION

This paper has presented the computational design of a novel, longitudinal flux induction heating system with a rectangular cross-section for uniformly heating thin sheets. Studies were performed using COMSOL® Multiphysics software to examine the effects of varying coil geometry on the temperature distribution. It was found that the most uniform temperatures resulted when the distance between coils was minimized. Additionally, the effect of varying the workpiece's vertical position was examined and found to have about $\pm 2\%$ difference from the case of a vertically centered workpiece. A bifurcation was found when varying the coil's width: both short and long widths resulted in the most uniform temperatures. However, shorter widths led to faster heating than longer widths. A similar phenomenon was observed when varying height.

The study has led to finding a cross-section geometry that yields a more consistent temperature distribution across the workpiece width for thin sheets. These results may be put toward the development of a new induction heating system for future experiments.

ACKNOWLEDGMENT

This work was supported by the Korea Institute of Machinery and Materials funded by the government of South Korea.

REFERENCES

- [1] Baker, R. M., 1944. "Heating of nonmagnetic electric conductors by magnetic induction - longitudinal flux". *American Institute of Electrical Engineers, Transactions of the*, **63**(6), pp. 273–278.
- [2] Egan, L. R., and Furlani, E. P., 1991. "A computer simulation of an induction heating system". *IEEE Transactions on Magnetics*, **27**(5), sep, pp. 4343–4354.
- [3] Lucía, O., Maussion, P., Dede, E. J., and Burdío, J. M., 2014. "Induction heating technology and its applications: past developments, current technology, and future challenges". *IEEE Transactions on Industrial Electronics*, **61**(5), pp. 2509–2520.
- [4] Paiva, R. M., Marques, E. A., da Silva, L. F., António, C. A., and Arán-Ais, F., 2016. "Adhesives in the footwear industry". *Proceedings of the Institution of Mechanical Engineers, Part L: Journal of Materials: Design and Applications*, **230**(2), pp. 357–374.

- [5] Yun, D., Kim, B., Oh, S. T., Kim, G. N., Jeon, H. K., and Shon, M., 2017. “Induction heating of adhesive for shoe manufacturing”. In IEEE CEFC 2016 - 17th Biennial Conference on Electromagnetic Field Computation.
- [6] Mondelaers, W., 1998. “Low-energy electron accelerators in industry and applied research”. *Nuclear Instruments and Methods in Physics Research Section B: Beam Interactions with Materials and Atoms*, **139**, pp. 43–50.
- [7] Chmielewski, A. G., Haji-Saeid, M., and Ahmed, S., 2005. “Progress in radiation processing of polymers”. *Nuclear Instruments and Methods in Physics Research, Section B: Beam Interactions with Materials and Atoms*, **236**, pp. 44–54.
- [8] Hamm, R. W., 2008. “Industrial Accelerators”. *Reviews of Accelerator Science and Technology*, **1**, pp. 163–184.
- [9] Mai, W., and Henneberger, G., 1998. “Calculation of the transient temperature distribution in a TFIH device using the impedance boundary condition”. *IEEE Transactions on Magnetics*, **34**(5), pp. 3090–3093.
- [10] Wang, Z., Huang, W., Jia, W., Zhao, Q., Wang, Y., and Yan, W., 1999. “3D Multifields FEM Computation of Transverse Flux Induction Heating for Moving-Strips”. *IEEE Transactions on Magnetics*, **35**(3), pp. 1642–1645.
- [11] Lupi, S., Forzan, M., Dughiero, F., and Zenkov, A., 1999. “Comparison of edge-effects of transverse flux and travelling wave induction heating inductors”. *IEEE Transactions on Magnetics*, **35**(5), pp. 3556–3558.
- [12] Blinov, K., Nikanorov, A., Nacke, B., and Klöpzig, M., 2011. “Numerical simulation and investigation of induction through-heaters in dynamic operation mode”. *COMPEL - The international journal for computation and mathematics in electrical and electronic engineering*, **30**(5), pp. 1539–1549.